We are IntechOpen, the world's leading publisher of Open Access books Built by scientists, for scientists

4,800
Open access books available

122,000
International authors and editors

135M
Downloads

Our authors are among the

154
Countries delivered to

TOP 1%
most cited scientists

12.2%
Contributors from top 500 universities

CLARIVATE ANALYTICS BOOK CITATION INDEX INDEXED

WEB OF SCIENCE™

Selection of our books indexed in the Book Citation Index in Web of Science™ Core Collection (BKCI)

Interested in publishing with us?
Contact book.department@intechopen.com

Numbers displayed above are based on latest data collected.
For more information visit www.intechopen.com

5

Molecular States of Electrons: Emission of Single Molecules in Self-Organized InP/GaInP Quantum Dots

Alexander M. Mintairov[1], James L. Merz[1] and Steven A. Blundell[2]
[1]*University of Notre Dame*
[2]*INAC/SPSMS, CEA/UJF-Grenoble*
[1]*USA*
[2]*France*

1. Introduction

Correlation between particles in finite quantum systems leads to a complex behavior and novel states of matter. One remarkable example of such a correlated system is expected to occur in an electron gas confined in a quantum dot (QD), where at vanishing electron density the Coulomb interaction between electrons rigidly fixes their relative positions like those of the nuclei in a molecule. Unlike real molecules, however, which have sizes and properties fixed by their chemical constituents, the size, shape and electronic density of such confined electronic structures, referred to as Wigner molecules (WM), can be varied experimentally using various combinations of semiconductor materials, types of nanostructures, numbers of electrons, electrostatic potentials and magnetic fields. Thus these WMs present a novel and compelling field for fundamental and applied research. So far, however, the properties of WMs and their underlying fundamental physics have been studied primarily by theory; what little experimental evidence there is for their existence consists only of measurements of charging energies and light-scattering spectra of GaAs/AlGaAs quantum dots created from modulation doped 2D-electron gas heterostructures.

Here we present the results of an experimental study of correlated states of electrons in a WM in self-organized InP/GaInP quantum dots. The unique properties of these QDs are their relatively large lateral size (~80-200 nm) and their ability to accommodate up to 20 electrons, providing electron density up to $2x10^{11}$ cm^{-2}. The dots have strong emission intensity which allows us using photoluminescence spectroscopy for their study. We used a high-spatial-resolution low-temperature near-field scanning optical microscopy (NSOM) having spatial resolution up to 30 nm in combination with a high magnetic field to resolve emission spectra of single QDs. Using emission spectra of single dots we observed crossover from a Fermi liquid to WM behavior at a critical density of $5x10^{10}$ cm^{-2}. A magnetic-field-induced molecular-droplet transition has been observed in the Fermi liquid regime. In the Wigner molecule regime we observed a rich vibrational structure of the emission spectra, which opens way to identify the electron arrangement in the WM. These results are discussed in detail and compared with existing literature data.

We also present theoretical calculations of electron correlation in quantum dots using an accurate configuration-interaction method employing a numerical mean-field basis set and analysis of vibrational modes in WMs using the classical limit.

2. Wigner localization in semiconductor quantum dots

A Wigner phase is a strongly correlated state of an electron system, in which electrons occupy separate sites forming a regular lattice. The possibility of crystallization of an electron gas at densities below a certain critical value (n_s) was predicted by Wigner in 1934 (Wigner, 1934). Experimentally such crystallization has been observed in two dimensional electron systems on the surface of liquid He (Grimes & Adams, 1979), in a GaAs/GaAlAs heterojunction (Andrei et al., 1988) and in Si (Pudalov et al., 1993) using detection of the metal-insulator transition.

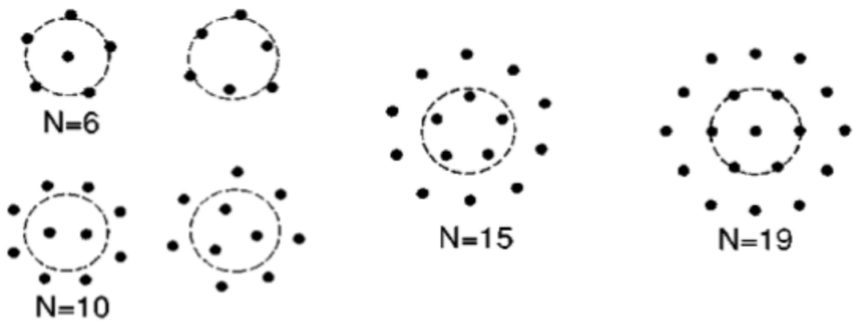

Fig. 1. Schematic view of the classical electron configurations in a parabolic potential for N=5, 6, 10, 15 and 19 (Bolton & Rössler, 1993).

The electrons confined in traps having volume >1/n_s form Wigner Molecules (WMs). Wigner localization of electrons in such traps formed by interface fluctuations is responsible for the quantum Hall effect in high mobility semiconductor heterostructures (Ilani et al., 2004; Laughlin, 1983). The Wigner localization regime can be realized in single electron transistors (SETs) using GaInAs/AlGaAs quantum dots (QDs) nano-fabricated from modulation doped quantum well structures (Kastner, 1993; Ashoori, 1996; Tarucha, 1996). Coulomb blockade measurements and theoretical analysis (Maksym et al., 2000; Reimann& Manninen, 2002; Szafran et al., 2003) have shown that a WM in such SETs can reveal a rich set of electron arrangements and spin states, which are controlled by the number of electrons present, and by an applied magnetic field. While electron arrangement in WMs will depend on the shape of the confinement potential and the number of electrons (N), theoretical analysis for the ideal 2D parabolic potential shows that in the classical approximation for systems having N<6, simple polygons are formed. The first nontrivial configurations are found for N=6 (see Fig.1). In addition to the ground state with five electrons surrounding a single electron at the center, metastable states and isomers at very similar energies exist, such as the 6-electron hexagon. Further, for N=10, the ground state is a "dimer" in the center with eight surrounding electrons. The hexagonal lattice of a Wigner crystal is not restored until N~200. In addition to the existence of metastable states, theory also predicts that the application of a magnetic field re-arranges the electron distribution in a QD and leads to specific phase transitions, which are called molecular-droplet transitions.

The effect of Wigner localization on electronic states is characterized by the dimensionless density parameter (Wigner-Seitz radius) $r_s=1/[a^*_B(\pi n)^{0.5}]$, where a^*_B is the effective Bohr radius and n is the average electron density in the plane of the dot. This parameter is approximately equal to the ratio of Coulomb-to-kinetic energy. It can also be expressed approximately via the parabolic (harmonic) potential frequency ω_0 via $r_s^3=1/[\omega_0^2 N^{0.5}]$], where ω_0 is expressed in units of effective Hartrees Ha*, and N is the number of electrons in the dot. For r_s<1, i.e. in the Fermi liquid regime (strong confinement potential), the electrons in a QD behave similarly to the electrons to the electrons in an atom and their energy spectrum for a 2D parabolic potential is $E_{K,L}= \hbar\omega_0(2K+|L|+1)$, with the K quantum number corresponding to the number of radial nodes in the electron wave function and L is the azimuthal quantum number. Note that this formula neglects the electron-electron interaction and is modified somewhat by the electronic mean-field potential. In the classical limit r_s>>10, and the electrons behave as point charges (Fig.1). According to the theoretical calculations for small numbers of confined electrons (say, up to 10), the onset of electron localization occurs gradually as r_s increases with partial Wigner localization in distinct WM geometries occurring already for r_s~4 (Egger et al., 1999).

The classical regime, resembling the point charge arrangements presented in Fig.1, was realized in the macroscopic experiment in which the electrons were represented by negatively charged (up to 10^9 electrons) metallic balls having 0.8 mm diameter and the trap (QD) was a positively charged cylindrical electrode having 10 mm in diameter (Saint Jean et al., 2001). For III-V semiconductor materials and in particular GaAs, the only semiconductor used so far for SETs, the effective Bohr radius having value a^*_B ~10 nm is relatively large and the classical regime requires potentials $\hbar\omega_0$<0.2 meV and large QD sizes >500 nm, which seems to be hardly achievable experimentally.

So far experimentally the signatures of formation of WMs were observed using a GaAs/AlGaAs heterostructure system with a two-dimensional electron gas. Using electrostatically-defined two-electron QDs having ω_0~5 meV and r_s~1.55, the existence of electron correlation was detected by identification of the singlet nature of the lowest excited state at finite magnetic field (Ellenberger et al., 2006). Light scattering spectra were used to observe spin and charge modes in nanofabricated QDs having two (Singha et al, 2010) and four (Kalliakos et al., 2008) electrons. These two and four electron dots have $\hbar\omega_0$~1.6 meV/r_s~3.4 and $\hbar\omega_0$~3.8 meV/r_s~1.7, respectively. The effect of formation of electronic molecules in these investigations was revealed from a fit of the observed energies using a configuration interaction approach.

In the present contribution we introduce InP/GaInP QDs as a natural WM system providing a great variety of electron occupation and sizes and, using high-spatial resolution nano-optical methods, we report the observation of emission of different types of WMs.

3. Excited states in Wigner molecules: Example for N=2 and N=6

3.1 Rovibrational states for N=2

In the Wigner localization regime the correlated state is characterized by the separation of the center-of-mass (c.m.) motion, having frequency ω_0, and a relative (rovibrational-spin) electron motion. According to the Kohn theorem this separation is an exact result for a

circular parabolic confining potential at any electron density (Jacak et al., 1998). For the simplest case of a two-electron molecule (2e-WM) the equations of motions allow an exact solution (Yannouleas&Landman, 2000). These solutions have shown that for r_s=200 the energy spectrum of 2e-WM has a well developed and separable rovibrational contribution exhibiting collective rotations, as well as stretching and bending vibrations:

$$E_{KL,kl}=Cl^2+(k+1/2)\hbar\omega_s+(2K+|L|+1)\,\hbar\omega_b, \quad (1)$$

where the rotational constant C≈0.037, the phonon for the stretching vibration has energy $1.75\omega_0$ and the phonon for the bending vibration coincides with that of the c.m. motion, i.e. $\omega_b=\omega_0$. Note that the bending vibration can itself carry an angular momentum $\hbar L$ and thus rotational angular momentum $\hbar l$ does not necessary coincide with the total angular momentum $\hbar(L+l)$. The calculations have shown that the molecule preserves its structure at r_s =3 ($\hbar\omega_0$~1 meV for GaAs), i.e. below the "theoretical" Fermi liquid to WM transition. Here the rotational sequence shows nearly equal spacing having value $\omega_0/2$ but the stretching vibration does not change.

3.2 Excited states of six-electron Wigner molecules

3.2.1 Configuration-interaction calculations of spin states

We used an accurate configuration-interaction (CI) method employing a numerical mean-field basis set to study the excitation spectrum of a six-electron WM (Blundell & Chacko, 2011). The CI method (Szabo&Ostlund, 1996; Blundell&Joshi, 2010) is more suitable for the systematic study of excited states than other methods such as Hartree-Fock-based methods and variational Quantum Monte-Carlo (which can treat only the lowest-energy state of a given symmetry). Dots with N ≥ 6 electrons in general have more than one classical isomer (see, for example, the [1,5] and [0,6] isomers in Fig. 1) and therefore isomeric states should form an important part of the phenomenology of excited states. Now, for a circularly

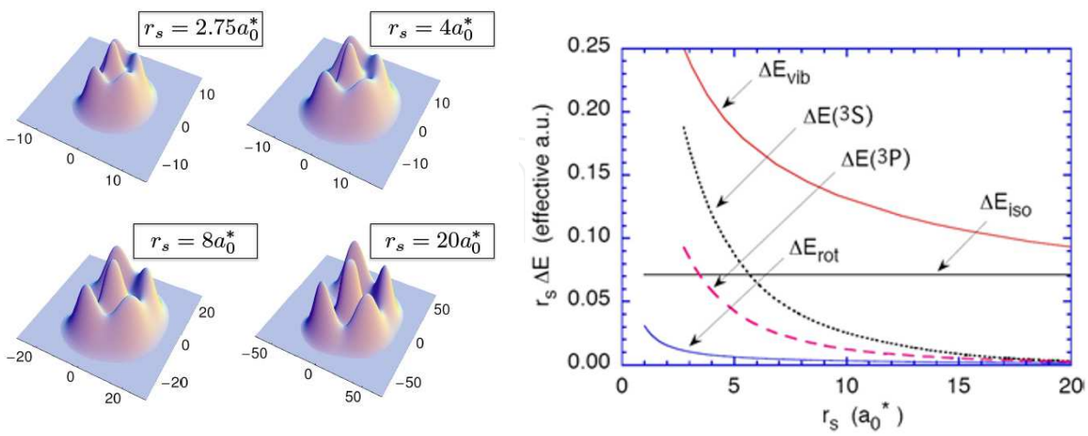

Fig. 2. Electron spatial pair correlation functions for r_s=2.75, 4, 8 and 20 (left) and excitation energies of the six-electron dot versus Wigner-Seitz radius r_s (right). The quantities ΔE_{rot}, ΔE_{vib}, and ΔE_{iso} are approximate rotational, vibrational, and isomeric excitation energies, respectively, inferred from a classical model (see text); $\Delta E(^3S)$ and $\Delta E(^3P)$ are excitation energies to the lowest ^3S and ^3P states calculated by CI. All excitation energies are scaled by r_s.

symmetric external potential and a state of definite L_z, the electronic density (in the "laboratory" frame) in 2D must also be circularly symmetric (Hirose&Wingreen, 1999) and in the Wigner limit the density therefore becomes a series of concentric rings (see, for example, Ghosal, et al., 2006). To reveal the Wigner localization, we therefore consider the internal many-body correlations by means of the electronic (charge-charge) pair-correlation functions (PCFs) $g(\mathbf{r}; \mathbf{r}_0)$ (Maksym, 1996; Reimann et al., 2000; Yannouleas&Landman, 2000). The quantity $g(\mathbf{r}; \mathbf{r}_0)$ is proportional to the conditional probability of finding an electron at the position $\mathbf{r}$ given that another (reference) electron is present at $\mathbf{r}_0$. Calculated $g(\mathbf{r}; \mathbf{r}_0)$ functions are presented for r_s = 2.75, 4, 8, and 20 in Fig. 2, from which it is seen that a partially correlated state is observed even at r_s = 2.75. Recall that r_s is expressed in units of the effective Bohr radius a_B*, where a_B* ≈ 8.7 nm for the InP/GaInP dots in our experiments.

Our calculations have shown that the evolution of the excitation energy of the lowest ^3S, ^5S, ^7S, and ^3P states relative to the ^1S ground state versus r_s yields approximately parallel straight lines on a logarithmic plot $6 \le r_s \le 10$, the excitation energy ΔE of these states being well fit by an expression of the form $\Delta E = c \exp(-m\, r_s)$, with $c(^3P)$ = 0.020 Ha*, $c(^5S)$ = 0.028 Ha*, $c(^3S)$ = 0.048 Ha*, $c(^7S)$ = 0.054 Ha*, and $m \approx 0.30\ (a_B^*)^{-1}$. The energy units Ha* here are effective Hartrees, with 1 Ha* ≈ 13.2 meV for the InP/GaInP dots used in our experiments.

3.2.2 Low-lying excitations in the classical limit

At large r_s the quantum excitation energy of a quasi-2D Wigner molecule may be written approximately in a way analogous to that for a planar molecule

$$E(\mathrm{P}) = E_{\mathrm{cl}}(\mathrm{P}) + L_z^2/(2I_P) + \Sigma_a\, [\Omega_a(\mathrm{P})(n_a+1/2)] + E_{\mathrm{spin}}, \tag{2}$$

where E_{cl}(P) is the classical electrostatic energy of isomer P, I_P is its moment of inertia, and n_a is the number of vibrational quanta in a normal mode with frequency Ω_a(P). The energy E_{spin} is the spin-spin interaction energy of the spins of the localized electrons. As an example of a typical rotational excitation energy, we note that the ground-state [1,5] isomer has a moment of inertia $I_P = 8.9\, r_s^2 N^{1/3}$, and it then follows using Eq. (2) that the S- to P-wave excitation energy is given in the classical limit by (in effective a.u.) $\Delta E_{\mathrm{rot}} = 0.0309\, r_s^{-2}$. Similarly, noting that the frequency of the first classical normal mode of the [1,5] isomer is $\Omega_1 = 0.650\omega_0$ (see below), we find that the excitation energy of one vibrational quantum in this mode is (in effective a.u.) $\Delta E_{\mathrm{vib}} = 0.415\, r_s^{-3/2}$. For isomeric excitations we found (Blundell &Chacko, 2011) $\Delta E_{\mathrm{iso}} = E_{\mathrm{cl}}$ (0, 6) – E_{cl} (1, 5) = $0.0714\, r_s^{-1}$. To clarify the role of rotational excitations, we show in Fig. 2 the classical estimate of the S- to P-wave excitation energy ΔE_{rot} as a function of r_s, together with the excitation energy calculated by CI (from the ^1S ground state to the lowest ^3P state, which is the lowest-lying P-wave state).

We also show a typical spin excitation energy $\Delta E(^3S)$, defined as the energy of the lowest ^3S state relative to the ^1S ground state, as calculated by CI. From Fig. 2, one sees that the smallest rotational excitation for r_s <10 is in fact somewhat larger than the classical estimate ΔE_{rot}. This is simply because a spin excitation is also involved. One also sees in Fig. 2 that for r_s < 6, the "spin" excitation energy (due to atomic-like exchange and correlation effects) is nominally comparable to the isomeric and vibrational energies. Thus, although at these values of r_s it is possible to find partial Wigner localization in a recognizable geometry, it is

not generally possible to discuss isomeric and vibrational excitations separately from spin excitations at these densities.

3.2.3 Vibrational modes

The classical normal modes for the [1,5] ground-state isomer are shown in Fig. 3. There are $2N - 1 = 11$ normal modes grouped into five doubly degenerate modes and one nondegenerate mode, which is a breathing mode at high frequency. The lowest frequency mode can be thought of as a dipolar oscillation of the central electron accompanied by a distortion of the outer ring. The third and fourth modes, at $\Omega=1.223\omega_0$ and $\Omega=1.314\omega_0$, correspond to quadrupole and octupole distortions, respectively, of the outer ring, with the central electron remaining fixed. The second mode is a collective dipolar oscillation of the c.m. of the system at frequency $\Omega=\omega_0$ (exactly), in which the whole structure remains undistorted during the oscillation. The existence of such a classical mode can be shown to be a general result for a system in a harmonic confining potential having an interaction depending only on the relative coordinates of the particles. The quantum mechanical analog of this result is the Kohn theorem, according to which under the same circumstances the c.m. motion decouples exactly from the "relative coordinates," and one can describe the system by a wave function in relative coordinates combined with oscillations of the c.m. in the harmonic confining potential. Note that the breathing mode of the six electron molecule has frequency $\Omega=1.732\omega_0$, which is nearly the same as the frequency of the breathing mode of the two electron molecule considered above.

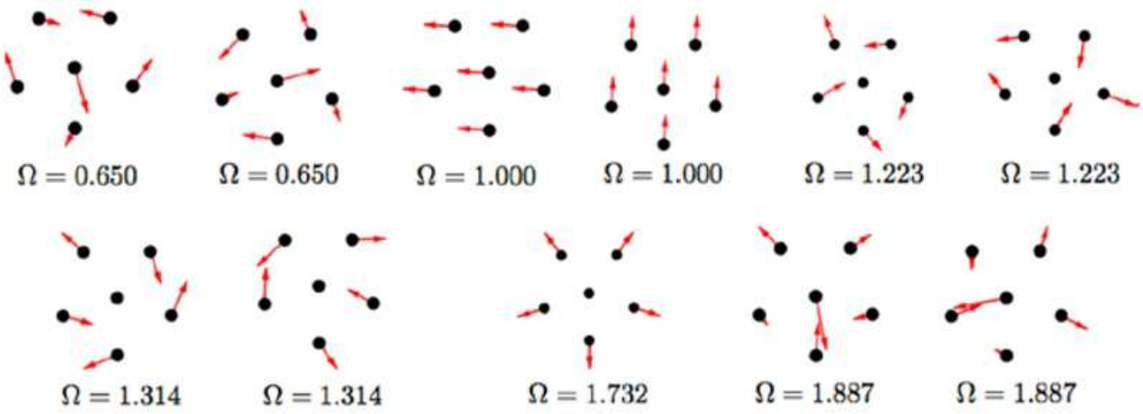

Fig. 3. Normal modes of the ground-state isomer of the classical six-electron dot. The normal mode frequency Ω is indicated as a multiple of the frequency of the parabolic potential ω_0.

3.3 Generalization to larger size N

We can use the classical arguments that work well for $N = 6$ to show that aspects of the same excited-state phenomenology apply to larger N as well. The classical model yields more than one isomer for $N = 6$ and for $N \geq 9$. We have used the "basin hopping" algorithm to generate and study the classical isomers in the size range up to $N = 20$. As N increases, the energy separation of isomers tends to become smaller. Thus the excitation energy $\Delta E_{iso}(N)$ for N electrons satisfies $\Delta E_{iso}(6) = 0.10\omega_0^{2/3}$, $\Delta E_{iso}(9) = 0.044\omega_0^{2/3}$ and $\Delta E_{iso}(19) = 0.013\omega_0^{2/3}$ (in effective a.u.). It is then generally the case that the first excited level (spin multiplet) for fixed L_z

at intermediate r_s is an isomer rather than a vibrational excitation of the ground state. We thus expect low-lying isomeric states to be a generic feature of the excitation spectrum of dots with $N = 6$ and $N \geq 9$ electrons at intermediate r_s values. Also, the rotational excitation energies ΔE_{rot} are generally found to be small compared to ΔE_{iso} and ΔE_{vib}, similar to Fig. 2 for $N = 6$.

4. InP/GaInP quantum dots as natural electronic molecules

4.1 Structural properties

Our InP/GaInP QD samples were grown by Metal-Organic Chemical Vapor Deposition (MOCVD) in a horizontal AIX200/4 reactor under pressure of 100 mbar. Trimethylgallium (TMGa), trimethylaluminium (TMAl) and trimethylindium (TMIn) metalorganic compounds were used as the group III element sources. Arsine (AsH_3) and phosphine (PH_3) were used as the group V element sources. (100) GaAs substrates misoriented by 2° towards the [110] direction were used. Initially a 50 nm-thick GaAs layer was deposited on the wafer. Then 50 nm thick $Ga_{0.52}In_{0.48}P$ (GaInP) lattice-matched with GaAs layer was grown. The QDs were grown at 725° C by depositing 7 monolayers (ML) of InP (Vinokurov et al,. 1999; Chu et al., 2009,). We studied the structures with uncapped dots and structures having GaInP cap layer thickness 5, 20, 40 and 60 nm.

The dot density (~2*10^9 cm^{-2}) and their sizes (base ~10-200 nm, height ~5-60 nm) were measured using atomic force microscopy (AFM) for the uncapped samples and transmission electron microscopy (TEM) for the capped samples. These data are presented in Fig.4a-d. A clear bimodal size distribution is seen from AFM images in Fig.4a consisting of large dots having size 100-200 nm and density 0.6x10^9 cm^{-2} and the small dots having sizes 10-70 nm and density 1.2x10^9 cm^{-2}. From TEM measurements a lens shape of the large dots was revealed (see Fig.4c and d). Due to a residual n-type doping of the GaInP layer in the MOCVD growth process (n~10^{16} cm^{-3}) the modulation doping of InP QDs occurs and they can contain up to 20 electrons (Hessman et al., 2001). Thus these QDs can represent natural WM and for dot sized 150-200 nm the r_s ~4 can be achieved for few electron dots. The electron density can be varied from 10^{10} up to 5x10^{11} cm^{-2} and thus these InP QDs offer much more flexibility in varying of WM parameters then "conventional" GaAs/AlGaAs QDs used in SETs (Singha et al, 2010).

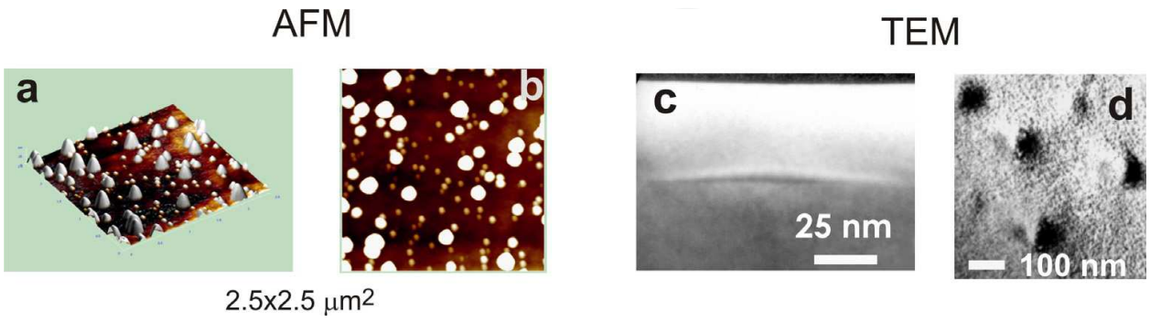

Fig. 4. Atomic force (a and b, size 2.5x2.5 μm^2) and transmission electron (c – plan-view, d – cross section) microscopy images of InP/GaInP QDs structures.

We estimated that our InP QDs can contain up to 10% Ga. Pure InP QDs can be grown by depositing nominally 0.5 ML of InP at growth temperatures 580 C and using in-situ annealing/growth interruption. Such growth conditions suppress Ga and In intermixing

and result in the pyramidal dot shape having base ~60 nm and height ~15 nm (Georgsson et al., 1995). Even smaller InP QDs having base 30 nm and height 7 nm were grown using 4ML InP deposition at 550 C (Ren et al., 1999).

In Fig.5a we present a cartoon showing the formation of a WM in our InP/GaInP QDs. Nine electrons come from the adjacent donor atoms located in the GaInP. The classical arrangement of a 9e-WM consists of eight electrons surrounding one electron at the center. The corresponding tentative band diagram of this QD is shown in Fig.5b. The barrier is formed by GaInP having band gap energy 1.97 eV (Janssens et al., 2003; Pryor et al., 1996). The "bandgap" of the QD material includes vertical confinement energy (~150 meV) and bandgap increase (~50 mev) due to Ga/In intermixing. We estimated the QD material bandgap to be ~1.7 eV, which is nearly 200 meV higher than the bandgap of InP. Due to strain effects and Ga/In intermixing we expect type-I band alignment between the QD and barrier material (Janssens et al., 2003; Pryor et al., 1997).

4.2 Photoluminescence of Wigner molecules

Under photexcitation an electron-hole pair is generated in the dot and it forms a trion with the central electron (see in Fig.5a). The formation of trions in a dilute electron gas is well established (Finkelstein et al., 1995) and thus we can assume that a radiative recombination of the trion also forms the photoluminescence (PL) spectra of the WM. The selection rules for radiative transitions of the trion involving the electron having spin ± 1/2 and the hole having spin ± 3/2 do not change the electron spin and thus only charge excitations are expected to dominate the emission spectra of the WM.

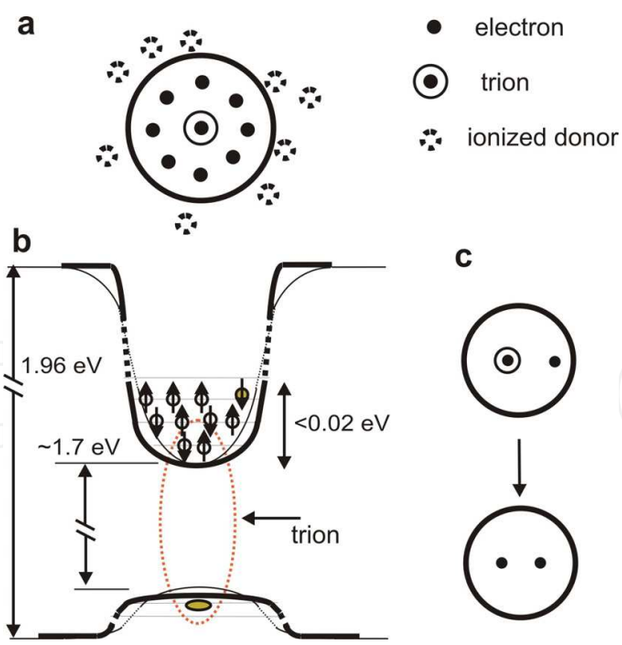

Fig. 5. Arrangement of electrons (classical positions) (a) and corresponding band diagram (b) of photo-excited nine-electron InP QD (base ~150 nm); classical positions of the trion and electrons in two electron WM before (upper) and after (lower) radiative recombination (c). Trion and adjacent ionized donors are also shown in a. Thick(thin) curves in b are the band diagrams for filled(empty) dot.

In Fig.5c we show classical positions of the trion and the electrons in the 2e-WM before (upper cartoon) and after (lower cartoon) the radiative recombination. It can be shown (Govorov et al., 2006) using the minimization of the classical energy of the electrons that the classical distance d^i_e of the electron to the dot center is a factor $\beta = m_{tr\omega 0tr}^2/m_{e\omega 0}^2$ larger than d^i_{tr}, the corresponding distance for the center of mass of the trion. This is because the trion confinement potential and corresponding harmonic frequency ω_{0tr}, is stronger than the electron confinement potential and corresponding harmonic frequency ω_0. In a similar way, we can determine the classical configuration of the two electrons left in the final state after photon emission. Their classical coordinate d^f_e in the ground state obeys relation $d^i_e > d^f_e > d^i_{tr}$ as seen in Fig.5c. The wave functions of the initial and final states are peaked at the classical coordinates and decay exponentially along the radial axis away from their peak positions (see for example Fig.2). Since $\beta \neq 1$, the classical coordinates for the initial and final states are different. This gives a coupling of the radiative recombination transition with vibrational modes of the WM which is the origin of the shake-up process in the photoluminescence of WM, to be discussed in the experimental part. Such "electron-phonon" coupling can be expressed via Huang-Rhys factors (Huang&Rhys, 1950).

From symmetry considerations one can see from Fig.5c that the annihilation of the trion induces stretching and center-of-mass distortion along the 2e-WM axis, thus generating the stretching and translation modes discussed above. Thus the emission spectra of a 2e-WM are expected to have contributions from the "zero-phonon" line (ZPL) and two sets of Stokes phonon replicas having energies $n\hbar\omega_0$ and $n\hbar 1.7\omega_0$, where n=1, 2, … . This is similar to the vibronic structure of conventional molecules.

Similar symmetry considerations based on classical electron arrangements shown in Fig.1 predict weak phonon Stokes emission for WM having a central electron, i.e. for N=6-9, and strong phonon Stokes emission for the two electrons at the center, i.e. N=2 and N=10-14.

5. The near-field scanning optical microscopy (NSOM) technique

5.1 Optical spectroscopy of quantum dots

For study of the effects of the electron localization in single InP/GaInP QDs we used the near-field scanning optical microscopy (NSOM) technique (Betzig&Trautman, 1993) in combination with magneto-PL spectroscopy. The basic principle of NSOM (Synge, 1928), providing a way to overcome the diffraction limit of light of conventional optics, is to use the coupling of the evanescent electromagnetic field and the radiative electromagnetic waves in the vicinity of a nano-probe placed near the boundary between two media. This principle was realized nearly three decades ago using nano-apertures (Lewis et al., 1984, Pohl et al., 1984), metallic (Fischer and Pohl ,1989) and dielectric (Coutjon et al 1989, Reddick at al., 1989) nano-tips, allowing nanometer-scale spatial resolution in optical experiments with a wide range of applications including experiments with single semiconductor QDs (Flack et al., 1996, Toda et al., 1996). The high spatial resolution, scanning ability and non-destructive character of the experiment in combination with a high magnetic field and time-resolved techniques, allows the use of NSOM to study structural parameters (Mintairov et al., 2001), the spin structure of exciton states (Ortner et al., 2003, Toda et al., 1998), the temporal coherence of the wave functions (Toda et al., 2000), and the mechanisms of carrier migration (K. Matsuda et al., 2000) and relaxation (Toda et al., 1999) in semiconductor QDs.

Achieving spatial resolution as high as 30 nm allows optical mapping of exciton wave functions in a single QD (Matsuda et al., 2003). Such spatial resolution is of the order of the electron separation in the Wigner localization regime and thus the NSOM technique opens the possibility to probe the position of the individual electrons in the electronic molecules. However, present GaAs/AlGaAs SET structures require relatively thick AlGaAs cap layers (~70 nm), which provides vertical modulation doping but does not allow achievement of spatial resolution below 200 nm (Mintairov et al., 2003). In contrast InP/GaInP QDs, having lateral modulation doping (see Fig.5b), can form a WM for cap layer thickness down to zero nm (see below). Thus the tip-QD distance separation can be zero and spatial resolution as high as 10 nm can be possible, as was demonstrated for single molecules (Hosaka& Saiki, 2001).

5.2 Experimental details

5.2.1 NSOM set up

For our low-temperature magneto-PL measurements we used an Oxford Instruments CryoSXP cryogenic scanner together with a liquid helium cryostat with a superconducting magnet providing magnetic fields up to 12 T. Shear-force tip-sample distance control and scanning are governed by a Vecco AFM controller from Digital Instruments, providing a scan range over an area of 3x3 μm^2 at 4.2K. For characterization of InP/GaInP structures at room temperature we used an NSOM-2000 system from NANONICs Inc. having a scan range 90x90 μm^2. The near-field photoluminescence (PL) spectra were taken in collection-illumination mode, i.e. laser excitation and PL emission collection using the same NSOM fiber probe. Emission was excited by the 488 nm line of an Ar ion laser and dispersed using a 270 mm focal length monochromator. The spectra were measured using a nitrogen-cooled CCD detector and 1200 gr/mm grating. Monochromatic NSOM images were measured using a 300 gr/mm grating and a GaAs photomultiplier working in the photon-counting regime with an accumulation time of 20 ms per pixel. Excitation power density was ~20-100 and 0.1-1 W/cm-2 for 300 and 10 K, respectively. The spectral resolution of the system is 0.2-0.4 meV. We measured spectra in a magnetic field up to 10 T. A quarter wave-plate and linear polarizer were used for the separation of right- and left-hand circular polarization.

5.2.2 NSOM probes

As near-field probes we used tapered single mode fiber tips. We used both metal coated and uncoated tips. Coated tips were prepared by electron beam deposition of metal (Al or Au in combination with Ti) having thickness ~50-200 nm. The physical structure of the aperture and its optical quality were controlled using scanning electron microscopy (SEM) imaging, visual observation of the light coming from the tip under a microscope with x100 objective, and by measuring its far-field transmission for 632.8 nm wavelength (HeNe laser). SEM images of typical near-field optical fiber probes are presented in Fig. 6a-f. The taper was prepared by using a pulling technique ((Lewis et al., 1984, Pohl et al., 1984). We used two pulling regimes in which the taper angle increases towards the tip end (see Fig.6a and b). Both regimes give tips (apertures) with diameters 200 nm and aperture angles 30-40^o (see Fig. 6c) but within a few micrometers from the aperture they have different taper angles. To make smaller apertures we used further chemical etching in a hydrofluoric acid solution (Otsu, 1998). We also use a focused ion beam milling technique to flatten the apertures (Fig.6f). The transmission of our metal coated fiber probes was 10-

^{4}-10^{-2}. Uncoated fiber tips provide an order of magnitude higher PL signals but in general they have poorer spatial resolution. Below, however, we will demonstrate an aperture less mode of uncoated tip in which spatial resolution is determined just by the apex diameter and thus can be as high as coated ones.

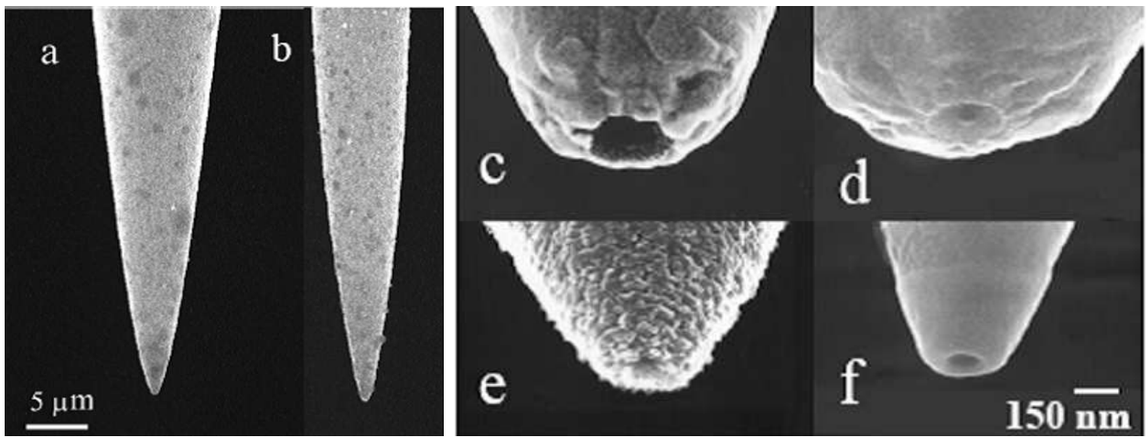

Fig. 6. SEM images of the near-field optical fiber probes: side view of the two types of tapers used (a, b); 45^{o} tilt images of apertures having diameters (nm) and coating: c - 280 and Au, d - 270 and Al, e - 60 and Al/Ti and f- 120 and Al. The apertures were prepared by pulling (c), etching (d-f) and FIB trimming (f).

5.3 NSOM imaging

Fig.7a-d presents our results of NSOM imaging of ~ 2 μm long section of a CdSe nanowire (NW) having diameter 40 nm taken with an uncoated fiber tip (Mintairov et al., 2010). It shows topographic (a) and monochromatic NSOM (b) images together with a set of twelve spectra measured along a 400 nm size central section of the wire (c) and a false-color wavelength-position plot of these spectra (d). Note that the topographic image is taken with the same fiber as the NSOM image. For further discussion we will denote the plot in Fig.7d as linear scan spectra (LSS) plot (image). Since we use accumulation time up to few seconds for each point of LSS image it can be considered as "static" image. The monochromatic NSOM image (see Fig.7b), taken at 20 ms per pixel, thus can be considered as a "dynamic" image.

In the topographic image (Fig.7a) the NW is seen as a vertical stripe having width ~100 nm. It has some distortions arising from the noise of the tuning-fork feedback control. We can estimate the width (W) and height (H) of the wire in the topography image to be W~100 and H~50 nm, respectively, and accounting for the fact that topographical height is equal to the wire diameter we can get value of the tip apex size to be TA=W-H~50 nm.

In the NSOM image (Fig.7b) the wire has a much larger width (~250 nm). It also reveals ~500 and ~100 nm intensity modulation along the wire. The fine scale modulation ~100 nm has the same scale as the topography. The nearly three times larger width of the NW in the NSOM image compared to the topography indicates an optical coupling between the wire and the tip before their physical contact, and reflects the "aperture less" nature of imaging using an uncoated tip. In such an aperture less regime the spatial resolution along the NW depends on the tip-wire distance and it is equal to the tip apex size (~50 nm for our tip)

when the tip and the wire are in contact. Thus the 100 nm size modulation of the emission intensity seen in the contact part of the NSOM image corresponds to an intrinsic uniformity of the NW emission of ~50 nm.

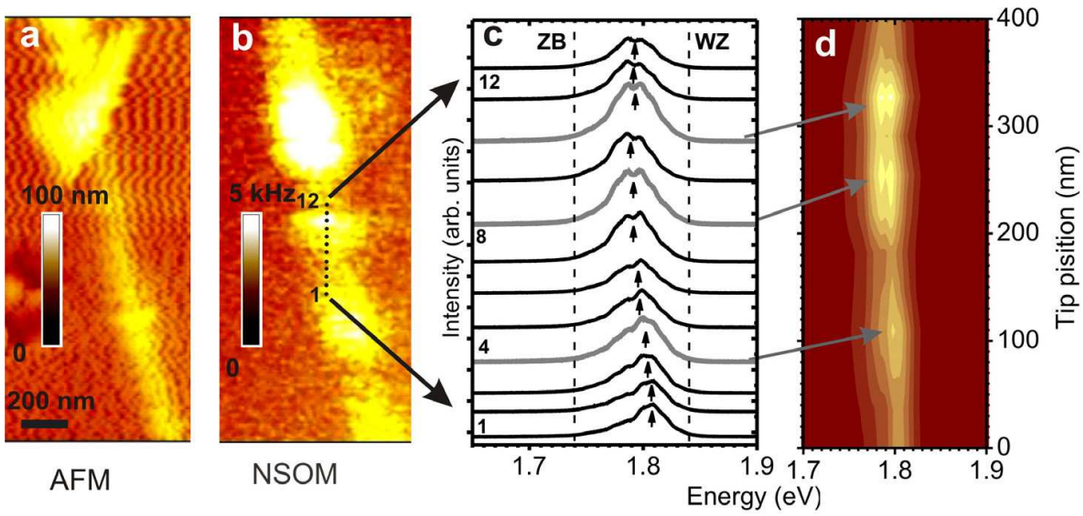

Fig. 7. Topography (a) and NSOM (b) images of NW1 at 50 K together with the set of twelve spectra taken during linear scan having length 400 nm (c) and their false-color wavelength-tip-position plot (d). Fiber tip positions for linear scan are marked by dots in (b). Image size in (a) and (b) is 0.8x2 μm^2. Detection energy in (b) is 1.8 eV

Comparison of Fig.7b and Fig.7c shows that variations of the intensity of the spectra follow the intensity variations in the monochromatic NSOM image. For example, the strong (weak) NSOM intensity in Fig.7b at points 9-11 (1-6) corresponds to strong (weak) spectra in Fig.7c taken at corresponding points. Some intensity variations seen in the spectra (like the intensity increase at point 8 and 4) are not observed in the NSOM image due to photon counting noise arising from the "dynamic" character of the image. Analysis of Fig.7c and d shows that intensity fluctuations are accompanied by changes of the spectral position and the width of the NW emission peak. For neighboring points separated by only 36 nm the changes of peak position and width by a few meV can be detected.

6. NSOM characterization and emission spectra of InP/GaInP structures

6.1 Room temperature NSOM imaging

Fig.8a-d shows the results of room temperature NSOM imaging of InP/GaInP QD structures having cap layer thickness d=0, 5, 20 and 60 nm. The images were taken at detection wavelength 750 nm. NSOM images of our structures (see inserts in Fig.8a and Fig.8b-d) show a set of bright spots having density ~20 μm^{-2} and size ~150-250 nm related to single QDs. Clearly-resolved single QD images are observed for 5 and 20 nm capped QDs as well as for the uncapped QDs. It is important to note the strong emission intensity for the uncapped QDs at room temperature. We believe that this is the first observation of such strong emission from uncapped QDs allowing ultra-high spatial-resolution. Accounting for the ~100 nm base of the QDs we estimated the tip apex size (spatial resolution) to be 25-75

nm. For a 60 nm cap the image contrast strongly decreases, which demonstrates the expected reduction of the spatial resolution (down to 150 nm) due to increased tip-dot separation. By positioning the tip on the bright spots we measured the spectra of individual InP/GaInP QDs at room temperature. Three such spectra for the uncapped sample presented in Fig.8a show that the spectra of single InP QDs at room temperature consists of a single band having wavelength in the range of 710-790 nm (1.75-1.56 eV) and halfwidth γ ~60 nm (~150 meV).

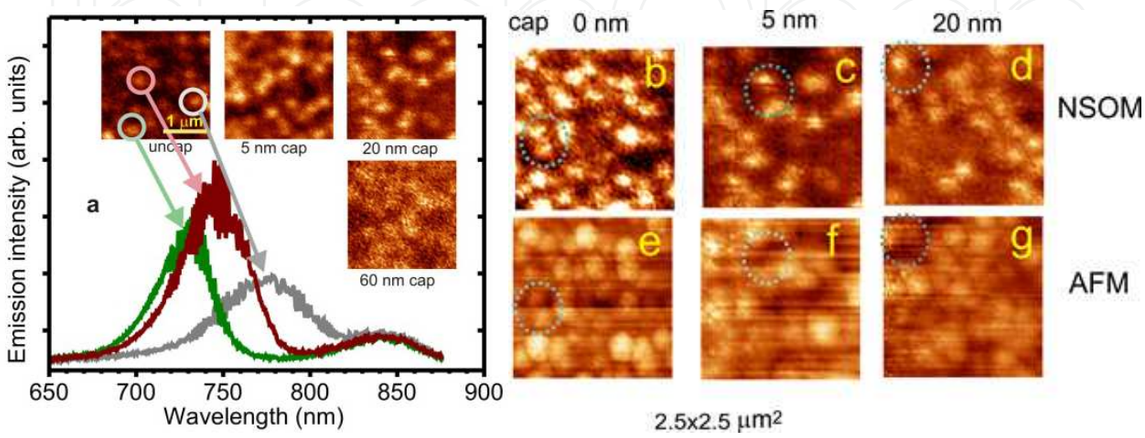

Fig. 8. Room temperature NSOM spectra (a) together with NSOM (b-d) and AFM (e-g) images (size 2.5x2.5 μm^2) of InP/GaInP QD structures having cap layer thickness (nm): 0 (b and e), 5 (c and f) and 20 (d and g). The ~500 nm diameter dashed circles in b-g outline the same area in the NSOM and AFM images. Inserts in 8a show NSOM images of the structures having cap layer thickness 0, 5, 20 and 60 nm.

In Fig.8b-g we present simultaneously measured NSOM (b, c and d) and AFM (e, f and g) images for d=0, 5 and 20 nm. The InP QDs having height 20-40 nm are clearly seen in the AFM image of the uncapped sample (Fig.8e). However the QD base observed is slightly (~50 nm) larger for the AFM image than in the NSOM image (see the encircled 1 dots in Fig.8b and e), which demonstrates the effect of electron localization. In the capped samples the QD location corresponds to the "valley" of the AFM images; this is seen by comparing the AFM and NSOM images (see the encircled dots for both the 5 and 20 nm cap) and the QD height decreases to 20-10 nm. Thus we observed the growth of the GaInP matrix material at the edges of the QDs. This together with the height reduction demonstrates additional growth control of the dot shape and thus confinement potential in InP/GaInP QDs.

We should also note that the use of the topographic images for the uncapped samples (see Fig.8b and e) allows the experimental determination of the size of the specific QD, which is one of the key parameters determining the electron correlation regime.

6.2 Low-temperature emission spectra

Fig.9 shows low-temperature (T=10 K) NSOM emission spectra of an InP/GaInP structure taken with spatial resolution ~200 nm at two fiber tip positions centred at two different QDs ($QD2_e$ and $QD3_m$) separated by 400 nm. (This notation will be clarified below). In the range

1.67-2.0 eV (740-620 nm) the spectra are dominated by the bands of the "central" dots, i.e. by $QD2_e$ in position 1 and by $QD3_m$ in position 2, having emission energy ~1.70 eV. Weaker bands of neighbouring dots located close to the tip edge are also seen at ~20 meV higher energy. The band shape of the large QDs reveals multipeak (manifold) structures, which will be discussed in detail below. The spectra also contain sharp lines observed in the range 1.85-1.95 eV, which are related to small InP QDs, and a broader band at 1.97 eV which is related to the GaInP matrix. The emission energy of our large InP QD is ~50 meV higher than the emission energy of the pyramidal InP QDs having base 60 nm, observed by other authors (Blome et al., 2000; Hessman et al., 2001), which indicates Ga/In intermixing. Using this energy difference we can estimate the value of the Ga composition of our InP QDs to be ~10%. Such intermixing resulting in significant increase of the dot size is favourable for the WM formation. Using low-temperature NSOM we measured the emission spectra of ~50 single InP QDs, allowing us to observe the effects of Wigner localization, which will be analysed below.

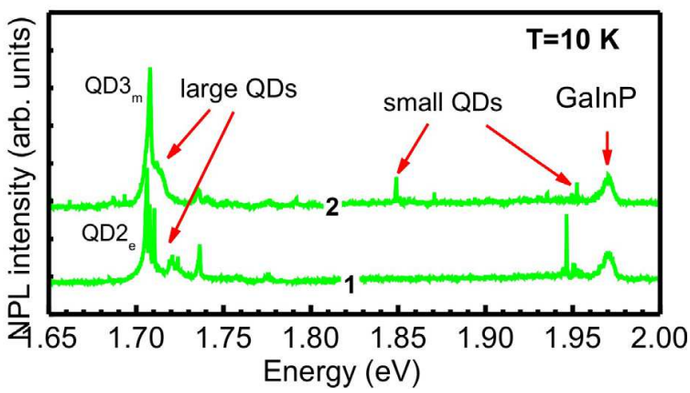

Fig. 9. 10K–NSOM spectra of InP/GaInP QD structures taken with spatial resolution 200 nm

7. Experimental study of Wigner molecules

7.1 Fermi liquid to Wigner molecule transition

Fig.10a shows an LSS plot, taken over a linear scan of 1.6 μm, for a 60 nm capped sample measured at T=10 K using a coated fiber having a 100 nm aperture. Four QDs denoted by $QD1_m$, $QD2_e$, $QD3_m$ and $QD4_e$ are observed in Fig.10a in the spectral range 1.72-1.68 eV. The spectra at tip positions 1 and 2 centered at $QD2_e$ and $QD3_m$ were shown in Fig.9 over a wider spectra range. Fig.10b-e compares the spectra of three large dots $QD5_m$, $QD1_i$, $QD2_e$ and a small lone dot $QD1_s$. The LSS image in Fig.10a demonstrates a drastic difference in the fine structure of the emission manifold of the dots having subscript m and e. This difference is also clear from the spectra of dots $QD5_m$ and $QD2_e$ in Fig.10c and e, respectively. In the m-type dots (further referred to as metallic) up to three components (s, p and d) of the emission manifold are observed and they have an energy splitting (ΔE) of ~4 meV and halfwidth (γ) of 3-5 meV. For the e-type dots (further referred to as excitonic) a fine structure of the s and p components consisting of several ultranarrow lines is clearly seen in Fig.10a, having γ<0.2 meV and ΔE as small as 1-2 meV. In Fig.10d we present the spectrum of a dot having a mixed structure consisting of few sharp lines and wider peaks. In contrast, for a small dot (Fig.10b) having ΔE >15 meV a single line related to a neutral

exciton is observed (Sugisaki et al., 2002). The manifold structure was also observed for ΔE values as large as 10 meV (Blome et al., 2000; Hessman et al., 2001) for pyramidal InP/GaInP QDs having base 60 nm.

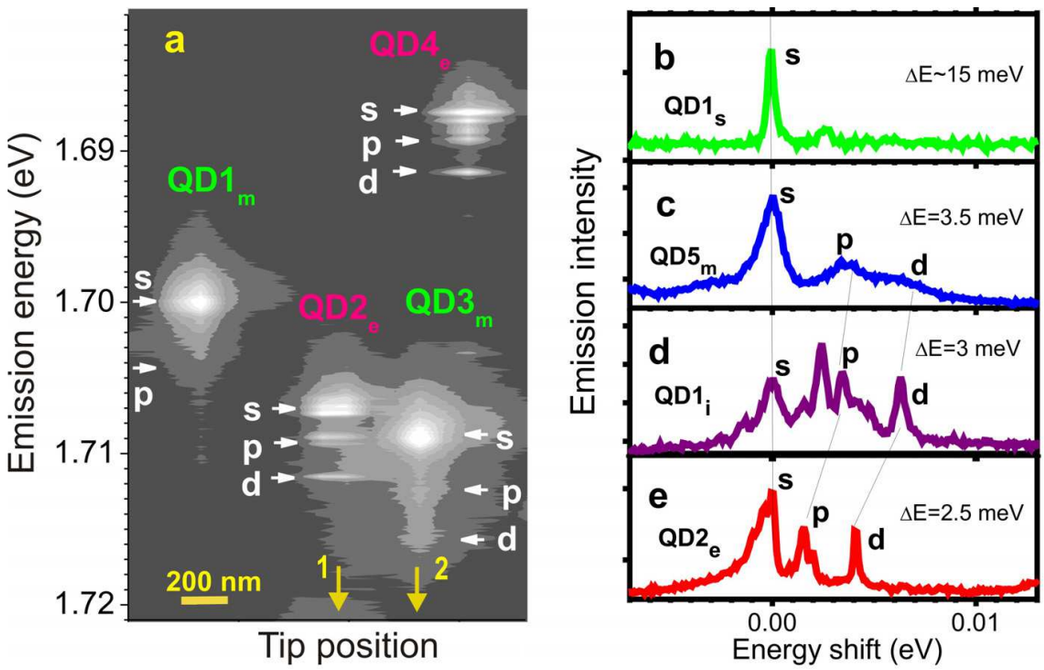

Fig. 10. Low-temperature (10K) NSOM LSS plot of InP/GaInP QD structure (a) and spectra of individual dots (b-e) The s-peak energy (in eV) in (b-e) is 1.9241 for $QD1_s$, 1.6994 for $QD5_m$, 1.7662 for $QD1_i$, and 1.7073 for $QD2_e$.

Our measurements of metallic QDs using a magnetic field discussed below have shown that the observed multi-peak structure of the emission spectra of InP/GaInP in Fig.10, c-e results from the filling of several electron shells. Here the spectral line shape is created by the radiative recombination of a photo-excited hole localized inside QD with electrons resulting from the "metallic character" of the dot; this is similar to the acceptor-related emission of a two-dimensional electron gas (2DEG) (Hawrylak, 1992). However in our QDs, i.e. a confined 2DEG, the spectral shape is determined by zero-dimensional confinement selection rules, and has maxima at the lowest s-state energy due to the s-state hole involved in the recombination process (see also the band diagram in Fig.5b), while in the 2DEG the spectral shape is determined by the density of the electronic states and is dominated by the high energy Fermi edge state (Hawrylak, 1992; Kukushkin et al., 1989).

The observed number of shells and the shell spacing allows us to estimate the number of electrons and the "effective" dot size, assuming a parabolic confinement potential (Jacak et al., 1998). The dots $QD5_m$ and $QD3_e$ in Fig.10c and e have spacing 3.5 and 2.5 meV, giving dot sizes ~90 and ~100 nm, respectively. They have three occupied s, p and d shells giving the possible number of electrons to be 7-12. Thus the electron density in these QD is ~5-$10x10^{10}$ cm^{-2}, which is similar to the density used in 2DEG GaAs/AlGaAs structures. Using the values of the dot size and the number of electrons we estimate r_s values of the InP QDs to be 1.5-2.5. Our observation of the narrowing of shell peaks and their fine structure for

excitonic dots indicates a formation of the excitonic/trion emission at a critical electron density at or below ~5x10^{10} cm^{-2}. Such a transition (from a broad Fermi sea emission to exciton and trion narrow lines) was observed in a 2DEG at higher densities (Finkelstein et al., 1995). Since the formation of the excitonic/trion emission in a many-electron system implies exciton/trion *localization* we can conclude that the multi-shell structure in these QDs reflects the formation of a Wigner molecule (WM). We believe this to be the first observation of a WM in a semiconductor QD.

7.2 Electron shell filling in the Fermi liquid regime

In Fig.11a and b we show the spectra of five metallic dots having varying ΔE and shell fillings. The QD7, QD8 and QD9 in Fig.11a have emission from three shells (~10 electrons) and show a progressive decrease of ΔE from 5.9 to 4.6 and to 3.5 meV, corresponding to sizes of the confining potential changing from ~65 to ~80 and to ~90 nm. On the other hand, QD10, QD7, and QD11 in Fig.11b show a progressive increase of the number of the shells from two for QD10 to three for QD7 and to four for QD11 (see spectra in a magnetic field below), thus demonstrating changes of the number of electrons from ~6 to ~20. The increase of electron numbers is accompanied by a decrease of ΔE, as expected.

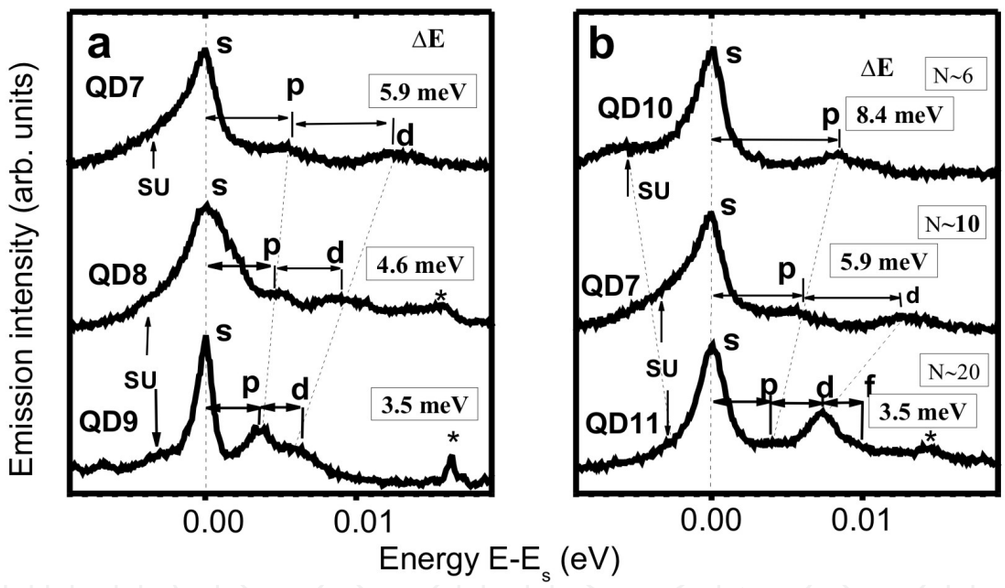

Fig. 11. Low-temperature (10K) NSOM spectra of five metallic single InP/GaInP QDs . The s-peak energy E_S is 1.7064, 1.6992, 1.6994 and 1.7041, 1.6981 eV for QD7, QD8, QD9 and QD10, QD11, respectively. Peaks * are contributions of neighboring QDs.

In addition to the shell peaks the spectra of single InP QDs display emission features related to so-called shake up or Auger processes denoted in Fig11a and b as SU. These features appear as low energy tails of the s-shell peak and for some dots they resolve into a separate band shifted by ~ΔE/2 (see QD9 and QD10). The scaling of the SU emission energy with ΔE is seen in Fig.11b. The SU emission occurs in many-electron systems when a recombining electron-hole pair excites surrounding electrons via the Coulomb interaction. In a 2DEG the SU emission appears at high magnetic fields via excitation of electrons into higher Landau

levels and related magneto-plasmons (Butov et al., 1992; Hawrylak&Potemski, 1997; Nash et al., 1993). SU emission from the excited states was also observed in an InAs QD ensemble (Paskov et al., 2000). In the Wigner localization regime one can expect a vibronic structure of the SU emission, as was discussed in section 4.2.

To probe Wigner localization in the metallic dots we used a magnetic field which effectively increases r_s by squeezing the electron motion. With increase of the magnetic field the WM is formed above the molecular-droplet transition at magnetic field >4T ((Maksym et al., 2000; Reimann&Manninen, 2002; Szafran et al., 2003). Details of this phenomenon follow.

7.3 Emission spectra of metallic dots in a magnetic field

7.3.1 Optically induced intra-dot magnetic field

Fig. 12a and b presents circular polarized emission spectra of QD11 and QD8 measured at magnetic field B=0, 1, 2 … 10T.

The s-shell band in Fig. 12a (QD11) at zero field is not polarized. With increasing magnetic field it becomes circularly polarized. The dominant emission of this band is σ⁺-polarized for B=1-3 and 9-10T and σ-polarized for B=5-7T. Zeeman splitting varies from +0.3 meV for 4T to -0.3 meV for 8T. The band shifts to higher energies with magnetic field.

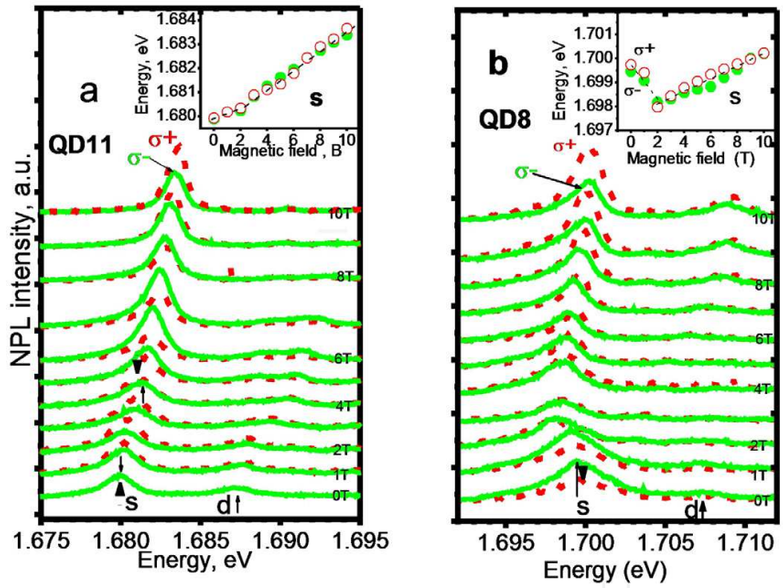

Fig. 12. Circularly polarized components (σ- - solid, σ+ - dotted) of emission spectra of QD11 and QD8 in magnetic field (0, 1, 2, …10 T). Inserts show position of the energy of the s-peak versus magnetic field. Dashed lines are drawn for clarity.

The s-shell band in Fig. 12b (QD8) shows different magnetic field behavior. First, unlike QD11, it has strong circular polarization and Zeeman splitting at zero magnetic field. Both circular polarization and Zeeman splitting disappear at 2T. Second, the band has a strong *low energy shift* (slope~0.8 meV/T) for magnetic fields 0-2T. For higher fields it has a high energy shift with a slope of 0.25 meV/T. Our observations of the circular polarization at zero magnetic field and negative magnetic field shift at B=0-2 T for QD8 reflect a strong

internal magnetic field. It arises from optical pumping of the nuclear spins (Brown et al., 1996; Maleinsky et al., 2007; Tratakovskii et al., 2007), inducing an internal magnetic field (B_{int}) of 2T which is anti-parallel to the external field. Such a field can induce the Wigner localization even at zero external magnetic field and thus using optical pumping gives additional control of WM formation.

7.3.2 Observation of the molecular-droplet transition

The measurements of the behavior of the multi-shell peaks in a magnetic field allow observation of a magnetic-field-induced phase transition of a WM using magneto-NSOM spectroscopy which is similar to that observed in Coulomb blockade measurements using nano-lithographically-defined GaInAs/AlGaAs QDs in a SET (Ashoori, 1996; Kastner, 1993; Tarucha, 1996). These measurements also confirm a shell type nature of an emission manifold of InP/GaInP QDs and estimate "valence" shell filling. In Fig.13a and b we show the unpolarized emission spectra versus magnetic field of QD8 and QD11 having ΔE=4.5 and 3.5 meV and N~10 and 20, respectively (see Fig.11a and b). In Fig.13c and d we compare the magnetic-field-induced shifts of the shell peaks for these QDs with the energy levels of the Fock-Darwin (FD) Hamiltonian. From Fig.13b and d one can see that for QD11 having larger size (i.e. smaller ΔE) than QD8, the f-shell peak is observed. Here the FD levels follow the experimentally observed shifts only for field up to 3T indicating filling of all f shell states, which gives electron number 19-20. At higher fields peak positions shift slightly to a lower energy and the d peak transforms to an x peak. This can indicate a transition of the electrons from the third (υ=2) to the second (υ=1) Landau levels. However, FD levels follow experiment only approximately and no distinct assignments of the shell peaks can be made at B>3T. We should point out that at 10T only a s-shell peak dominates the spectra and all other shells strongly suppressed.

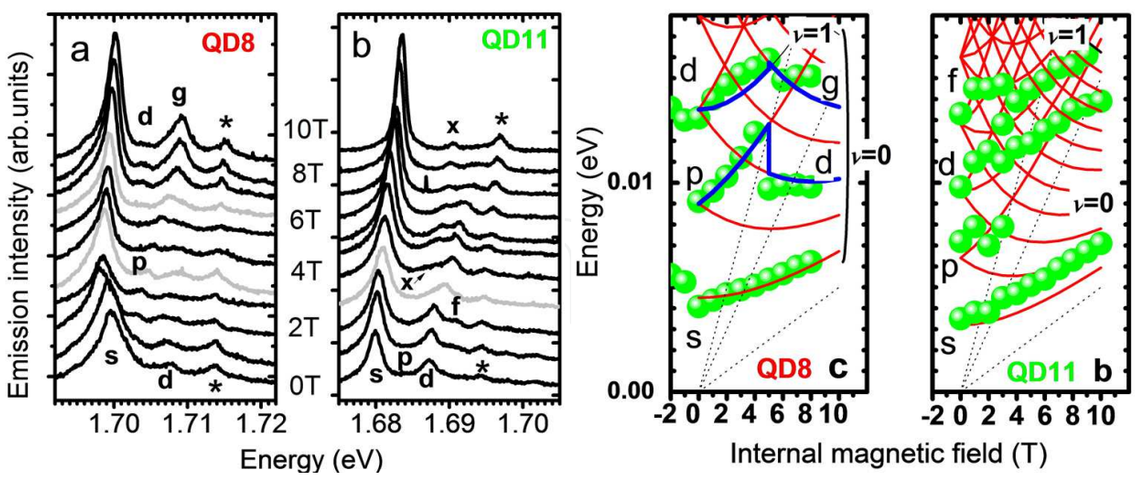

Fig. 13. Near-field spectra at 10 K representing shell structure (peaks s-g) of QD8 (a) and QD11 (b) at magnetic fields 0, 1,..,10T. Peaks * are contributions of neighboring QDs. Energy shift of emission peaks of QD8 (a) and QD11 (b) versus magnetic field (solid circles) are shown in (c) and (d), together with calculated Fock-Darwin energy levels (solid curves) and Landau levels υ=0 and 1 (dashed lines). In (c) and (d) the abscissa is the net *internal* magnetic field.

For QD8 (Fig.13a and c) the observed magnetic-field-induced shell shifts follow the FD energy levels remarkably well. Here two magnetic-field induced transitions are observed. The first transition occurs at B=2T arising from an internal magnetic field (B_{int}) of 0T which was discussed above (see Fig12.b). In the unpolarized spectra presented in Fig.13a, B_{int} is responsible for the shift to lower energy of the s- and d-shell peaks at B<2. For B>2 (B_{int}>0) the peak positions shift to increasing energy (see Fig.13c). In the range B=2-7 T (B_{int}=0-5 T) the p-shell peak appears. At B>7 T (second transition; B_{int}=5 T) the p-shell peak transforms into a d-shell, and d into g-shell. As can be seen from Fig.13c the second transition (at 7T) corresponds to transition of electrons from the second (υ=1, p/d-shells) to the first Landau level (υ=0, d/g-shells). Such a transition was previously observed in the magnetic field dependence of Coulomb blockade and can be described as a molecular-droplet transition (Oosterkamp et al., 1999). It arises from formation of a maximum-density-droplet at B=2, and its decomposition is accompanied by a WM formation at B>4 T (Maksym et al., 2000; Reimann& Manninen, 2002; Szafran et al., 2003). In the spectra the WM formation at a high magnetic field corresponds to a strong increase of the intensity of the g-shell peak (in contrast to QD11).

7.4 High-spatial resolution NSOM imaging

We used the uncapped structure to perform ultra-high-spatial resolution imaging and spectroscopy of InP/GaInP QDs using uncoated fiber probes working in an apertureless regime. In Fig.14a and b we present monochromatic 5K-NSOM images (detection energy 1.713 eV) taken for the same area (size 500x500 nm^2) in two separate scans. Fig.14c and d shows an LSS plot for the dashed line along the dot center shown in Fig.14a, and seven selected spectra from this scan (denoted 1-7), respectively. Fig.14e shows classical positions of the electrons and the trion for nine (cartoons I and II) and ten (cartoon III) electron WMs. In the NSOM image in Fig.14a and b in addition to the bright resonant QD denoted Qa (emission energy 1.713 eV), two weaker non-resonant QDs denoted Qb and Qc (emission energy 1.701 and 1.695 eV, respectively) appear in the images. Resonant Qa dot has ΔE=5.5 meV and three shells are filled, as can be seen from the spectra in Fig.14d. The image of Qa has size ~120 nm and it reveals a strong (up to 50%) intensity fluctuation on a length scale ~30 nm, which is of the order of the single electron separation in a WM in the classical limit. We determined, using LSS in Fig.14c and d, that the photon counting detection noise only partly contributes to the spatial intensity fluctuation in Fig.14a and b (note that photons are counted only for 20 ms in monochromatic imaging). In the image in Fig.14c plotted from spectra measured by a CCD with accumulation time 1 s we observed similar spatial fluctuations of the emission intensity. From Fig.14c and d it is seen that intensity fluctuations are accompanied by changes of the SU-part of the emission spectra and by the spectral diffusion of a few meV. Spectral diffusion indicates the effects of rearrangement of the charge distribution inside and/or around the QDs under near- field excitation. It is seen from Fig.14c and d that for positions 1, 2, 4 and 7 the SU-emission consists of two peaks SU1 and SU2, having energy shift from the s-peak of ~3 and 5 meV, respectively. For positions 3 and 6 the SU1 peak reveals a splitting of ~2 meV, and for position 5 a SU0 peak having energy shift ~2 meV appears. For position 5 the intensity of the SU0 emission peak is very strong: it is nearly the same intensity as the intensity of the s-peak. Using the analysis of the "electron-phonon" interaction discussed in section 4.2 and WM excited states discussed in section 3 we suppose that the SU1 and SU2 peaks can

be related to the translational and breathing vibrational modes and that the splitting of the SU1 peak is related to a other normal mode of a 9e-WM. We assign the SU0 peak to isomeric excitation of a 10e-WM. The appearance of the different (from translational and breathing) modes for positions 3 and 6 can be explained by photoexcitation at the edge of the dot, in which recombination of an "edge" trion generates the WM rotational motion (cartoon II in Fig.14e). For photoexcitation at the center of the dot (position 4), no rotations are generated by symmetry (see cartoon I in Fig.14e). Positions 1 and 7 are non-contact positions for which the photexcitation can be considered uniform. We can expect that for such excitation the emission is generated by the trion bound to the central electron. We also suppose that the enhanced coupling to the vibrational mode arises in a 10e-WM due to the formation of a two-electron isomeric arrangement at the center see Fig.14e, cartoon III). We obtained further evidence of vibronic structure of the SU-emission from analysis of spectra of the excitonic dots.

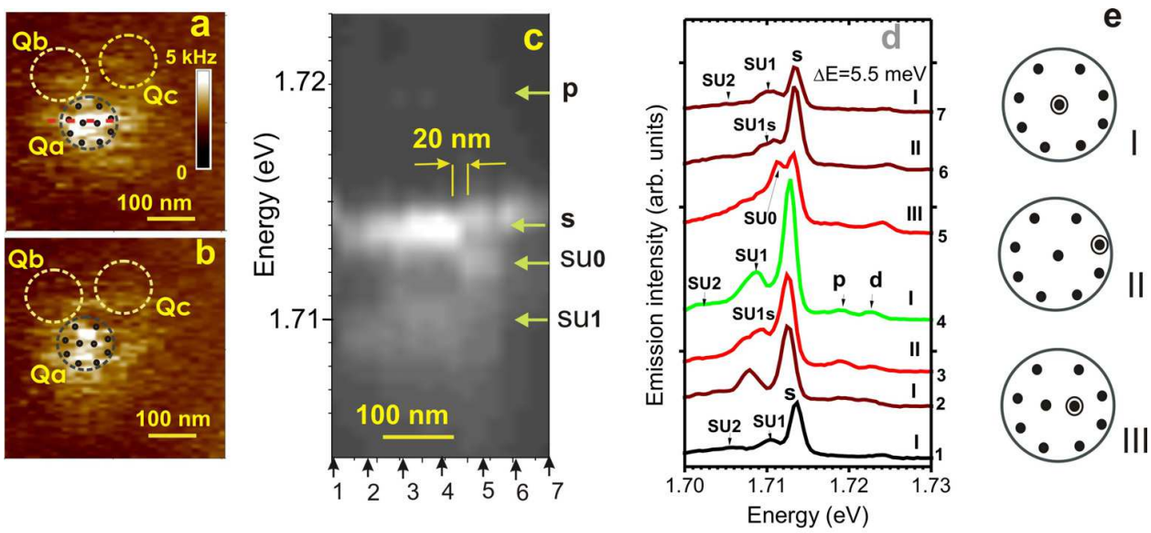

Fig. 14. High-spatial resolution NSOM measurements of InP QDs at 5 K: (a and b) monochromatic NSOM image, (c) false-color LSS-plot for a scan along the QD (see dashed horizontal line in a); (d) seven selected spectra from LSS (see vertical arrows at the bottom of c) from the linear scan; (e) classical arrangements of electrons and trion in photoexcited state of nine (upper and central) and ten electron WMs. In (a) and (b) Qa, Qb and Qc dashed large circles outline different QDs, while the small circles in dot Qa represent possible WM electron positions.

7.5 Emission spectra of Wigner molecules

Fig. 15a-d show spectra of four excitonic dots ($QD2_e$, $QD3_e$ $QD4_e$ and $QD5_e$) having different intensity distributions of the shell and SU peaks. The ΔE for these dots have values between 1 and 1.9 meV. Three shell peaks are observed for $QD2_e$, $QD3_e$, and $QD4_e$ and two for $QD5_e$. The p-shell peaks for $QD2_e$ and $QD4_e$ reveal two components having splitting 0.4-0.5 meV whereas no components are observed for $QD3_e$ and $QD5_e$. The p- and d-shell peaks are strong for $QD2_e$, $QD4_e$ and $QD5_e$ and weak for $QD3_e$. The intensity of the SU emission is strong for $QD2_e$, $QD3_e$ and $QD5_e$ and very weak for $QD4_e$. The energy shift of the SU peaks

in units of ΔE is equal to 0.2, 0.4 and 1.5 for $QD2_e$, $QD3_e$ and $QD5_e$. The right inserts in Fig. 15 shows our suggestions for the WM structure, which could explain the observed differences in the spectra.

We suppose that $QD2_e$, $QD3_e$, $QD4_e$, and $QD5_e$ have ten, ten, nine, and two electrons, respectively. Three of the electrons in $QD2_e$ are centrally located, whereas only two are centrally located in $QD3_e$. For $QD2_e$ the optical transition interacts equally with all three electrons, giving the high intensity of the p- and d-shells. The SU structure arises from the interaction with the other WM arrangement ($QD3_e$) having two central electrons, and the energy 0.2ΔE is the splitting between these arrangements, which is the energy difference of the isomeric excitations. The intensity distribution for $QD3_e$ is similar to the metallic dot Qa in Fig.14 (see also Fig16b below).

The $QD4_e$ dot must have electron number between 7 and 9 since the d shell is populated and the existence of the central electron suppresses the SU emission. The SU structure of $QD5_e$ allows us to assume that this is a two electron QD. This is supported from our analysis of the SU peak structure presented in Fig.16a.

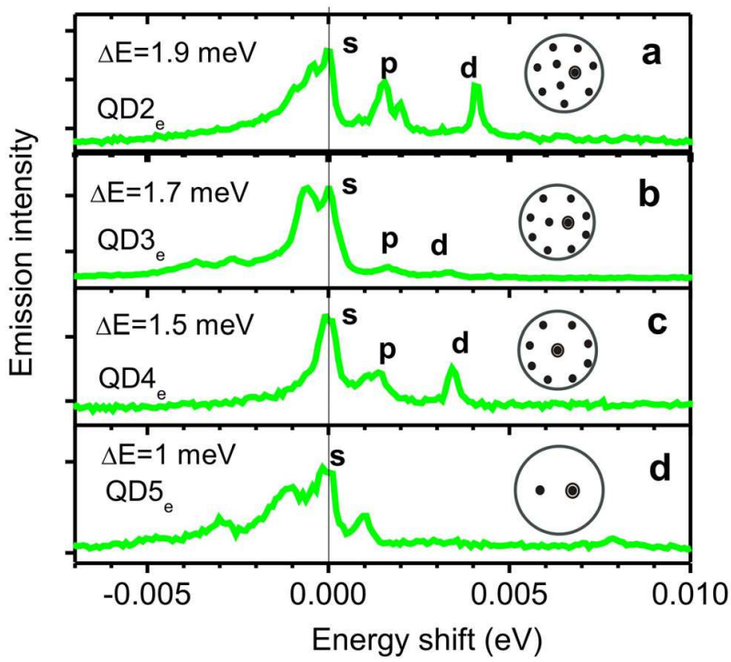

Fig. 15. Emission spectra of excitonic QDs molecules at 10 K. Right inserts show possible classical positions of electrons and trion of corresponding WMs in the excited state. E_s energy (in eV) is 1.7073 for QD_{2e}, 1.766 for $QD3_e$, 1.687 for $QD4_e$ and 1.7438 for $QD5_e$

7.5.1 Vibronic structure of a two-electron Wigner molecule

We use six Gaussian peaks to model the SU structure of this $QD5_e$ (see Fig.16a). Our analysis has shown that the energy of these peaks can be grouped in two sequences – one is n*ΔE and the other is n*1.5ΔE, or $n\omega_0$ and $n*1.5\omega_0=n*\omega_S$, where n is an integer. These energies are

naturally assigned to bending and stretching vibrations of a 2e-WM (see Eq. 1), which according to the theoretical calculations have values ω_0 and $1.7\omega_0$. The smaller value of the frequency of the stretching vibration observed experimentally ($1.5\omega_0$ instead of $1.7\omega_0$) can result from deviations of the real confinement potential from the ideal 2D potential. The anti-Stokes peak ω_0 arises from the thermal activation and its relative intensity is well described by the thermal factor exp(-ΔE/kT), which for T=10K is equal to 0.3. From the intensities of the peaks we can estimate Huang-Rhys factors for bending and stretching vibrations to be ~0.2 and ~0.1.

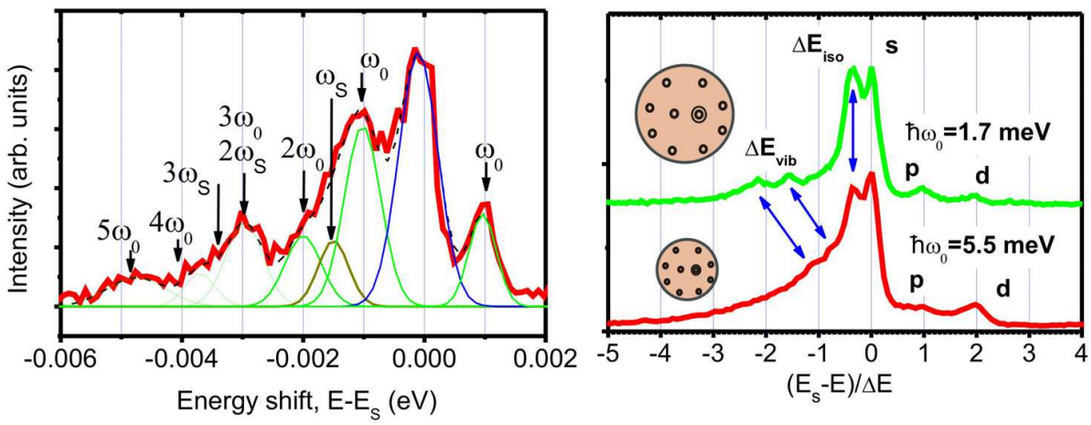

Fig. 16. Gaussian contour decomposition of emission spectra of $QD5_e$ (a) and comparison of emission spectra of two QDs having shell splitting ΔE=1.7 and 5.5 meV (b). The horizontal axis in b has reduced units $(E_s\text{-}E)/\Delta E$.

7.5.2 Size-dependent structure

Fig. 16b shows the comparison of the emission spectra of the metallic and the excitonic dots having similar intensity distributions of the SU peaks. These are the Qa dot (lower spectrum in Fig. 16b), the spectrum of which is also shown in Fig.14d for tip position 5, and the QD3e dot (upper spectrum), the spectrum of which is shown in Fig.15b. The shell splitting of these two dots is 1.7 and 5.5 meV, which corresponds to sizes 120 and ~70 nm, respectively. We suppose that these two dots have the same electron occupation equal to ten, which corresponds to r_s~2 and ~1.2. The horizontal axis in Fig.16b is in reduced units $n=(E_S\text{-}E)/\Delta E$ or $n=(E_s\text{-}E)/\hbar\omega_0$ and from Fig.16b a very good coincidence of the spectral shape is seen. This coincidence is remarkable, accounting for a nearly three times difference in the absolute spectral range, which is equal 15.3 and 45.5 meV for QD3e and Qa, respectively, for n values from -5 to 4 in Fig.16b. These dots have a strong SU peak having the same intensity as the intensity of the "zero-phonon" line, i.e. the s-peak. The weaker structure also observed near n=2 for QD3e and n=1 for Qa. The SU peak can be assigned to the isomeric excitation between the ground isomer having [2, 8] classical electron geometry and excited isomer having [3,7] geometry. This follows from the fact that this is the only excitation which linearly scales with r_s (see Fig.2). The weaker structure does not scale with r_s and it shows shrinkage of the energy. Such shrinkage is expected for a transition from partial Wigner localization to Fermi liquid discussed in section 3.1 for 2e-WM. For the excitonic dot the

energy of the weak structure is ~$2\hbar\omega_0$, which fits well to the high frequency vibrational modes. These modes include the breathing mode, having frequency $1.7\omega_0$ (see Fig.3). Reduction of this energy down to $\hbar\omega_0$ for a metallic dot reflects the loosing of the molecular character of the electron distribution for r_s~ 1.2 and failure of the classical approximation. In this Fermi liquid regime the electron motion is described only by translation vibration having frequency ω_0.

We should also point out the stronger contribution of p- and d-shell peaks in the smaller Qa dot, which reflect stronger overlap of hole and electrons wave functions.

8. Conclusions

We presented the results of an experimental (photoluminescence) study of correlated states of electrons in a WM in self-organized InP/GaInP quantum dots. The unique properties of these QDs are their relatively large lateral size (~80-200 nm) and their ability to accommodate up to 20 electrons, providing electron density up to $2x10^{11}$ cm^{-2} and strong emission intensity. Using high-spatial-resolution low-temperature near-field scanning optical microscopy (NSOM) having spatial resolution up to 30 nm in combination with a high magnetic field, we were able to resolve emission spectra of single QDs, and to observe crossover from a Fermi liquid to WM behavior at a critical density of $5x10^{10}$ cm^{-2}. A magnetic-field-induced molecular-droplet transition has been observed in the Fermi liquid regime. In the Wigner molecule regime we observed a rich vibrational structure, which opens the way to identify electron arrangement in WMs. Further experiments are in progress.

9. Acknowledgment

Development of the NSOM technique was supported by a National Science Foundation NIRT grant No. ECS-0609249. The authors wish to thank Nikolay A. Kalugnyy, Vladimir. M. Lantratov, Sergei A. Mintairov and Dmitrii A. Vinokurov from the Ioffe Physical-Technical Institute (St. Petersburg, Russia) for growth InP/GaInP structures. The authors wish to thank Alexei Vlasov and Tatiana Prutskih for making fiber tips and for help in NSOM measurements.

10. References

Andrei, E.Y.; Deville, G.; Williams, F.; Paris, I.B. & Etienne, B. (1988). Observation of Magnetically Induced Wigner Solids, *Physical Review Letters*,Vol.60, No.26 ,(27 June), pp.2765-2768

Ashoori, R.C. (1996). Electrons in artificial atoms, *Nature,* Vol.379, (1 February), pp.413-419

Betzig, E. & Trautman, J. K. (1992). Near-Field Optics: Microscopy, Spectroscopy, and Surface Modification Beyond Diffraction Limit, *Science* Vol.257, (10 July), pp. 189-195

Blome, P. G.; Wenderoth, M.; Hubaner, M. & Ulbrich, R. G. (2000). Temperature-dependent linewidth of single InP/$Ga_xIn_{1-x}P$ quantum dots: Interaction with surrounding charge configuration, *Physical Review B,* Vol.61, No.12, (15 March) pp.8382-8387

Blundell, S. A. & Chacko, S. (2011). Excited states of incipient Wigner molecules *Physical Review B,* Vol.83, No.19, (31 May) pp.195444-11

Blundell, S. A. & Joshi, K. (2010). Precise correlation energies in small parabolic quantum dots from configuration interaction, *Physical Review B,* Vol.81, No.11, pp.115232-1-11

Bolton, F. & Rössler, U. (1993). Classical model of a Wigner crystal in a quantum dot, *Superlattices and Miucrostructures*, Vol.13, No.2 (March) pp.139-145

Brown, S. W.; Kennedy, T. A.; Gammon, D. & Snow, E. S. (1996). Spectrally resolved Overhauser shifts in single GaAs/$Al_xGa_{1-x}As$ quantum dots, *Physical Review B, Vol.*54, No.24 (15 December) pp.R17339-R17342

Butov, L. V.; Grinev, V. I. ; Kulakovskii, V. D. & T. G. Anderson (1992) Direct observation of magnetoplasmon-phonon coupled modes in the magnetophotoluminescence spectra of the two-dimensional electron gas in $In_xGa_{1-x}As$/GaAs quantum wells, *Physical Review B,* Vol.46, No.20 (15 November) pp. 13627-13630

Chu, Y.; Mintairov, A. M. ; He, Y.; Merz, J. L.; Kalyuzhnyy, N. A.; Lantratov, V. M.& Mintairov S. A. (2009). Lasing of whispering-gallery modes in asymmetric waveguide GaInP micro-disks with InP quantum dots, P*hysics Letters A*, Vol.373, 1185-1188

Coutjon, D.; Sarayeddine, K.& Spajer, M. (1989). Scanning tunneling optical microscopy, *Optics Communication,* Vol.71, No.1,2 (1 May) pp.23-28

Egger, R.; Häusler, W.; Mak, C. H. & Grabert, H. (1999). Cossover from Fermi Liquid to Wigner Molecule Behavior in Quantum Dots *Physical Review Letters* 82 3320

Ellenberger, C. Ihn, T. Yannouleas, C Landman, U. Ensslin, K. Driscoll, D. & Gossard A. C. (2006) Excitation Spectrum of Two Correlated Electrons in a Lateral Quantum Dot with Negligible Zeeman Splitting, *Physical Review Letters* 96, 126806

Finkelstein, G.; Shtrikman, H. & Bar-Joseph, I. (1995). Optical Spectroscopy of Two-Dimensional Electron Gas near the Metal-Insulator Transition, *Physical Review Letters* Vol.74, No.6 (6 February) pp.976-979

Fischer, U. C. & Pohl, D. W. (1989). Observation of Single-Particle Plasmons by Near-Field Optical Microscopy, *Physical Review Letters,* Vol.62, No.4 (23 January), pp.458-461

Flack, F. ; Samarth, N.; Nikitin, V.; Crowell, P. A.; Shi, J.; Levy, J.& Awschalom, D. D. (1996). Near-field optical spectroscopy of localized excitons in strained CdSe quantum dots, *Physical Review B,*Vol.54, No.24 (15 december) pp.R17312-R17315

Georgsson, K.; Carlsson, N.; Samuelson, L.; Seifert, W.& Wallenberg L. R. (1995) Transmission electron microscopy of the morphology of InP Stranski-Krastanov islands grown by metalorganic chemical deposition *Appl. Phys. Lett.* Vol.67, No.20 (13 November) pp. 2981-2982

Govorov, A. O.; Schulhauser, C.; Haft, D.; Kalameitsev, A. V.; Chaplik, A.; Warburton, R. J.; Karrai, K.; Schoenfeld, W.; Garcia, J. M.& Petroff P. M. (2002). Magneto-optical properties of charged excitons in quantum dots, (26 February, 2002) Available from arXiv:cond-mat/0202480 v1

Ghosal, A.;. G¨uc¸l¨u, A. D.; Umrigar, C. J.; Ullmo, D. & Baranger H. U. (2006). Correlation-induced inhomogeneity in circular quantumdots, *Naure Physics.* Vol.2, No.5 (23 April) pp. 336-340

Grimes, C.C.& Adams, G. (1979) Evidence of Liquid-to-crystal Phase Transition in a Classical Two-Dimensional Sheet of Electrons *Physical Review Letters Vol.*42, No.12, (19 March) pp.795-798

Hawrylak, P. *(*1992). Many electron effects in acceptor-related radiative recombination of quasi-two-dimensional electrons, *Physical Review B,* Vol.45, No.8 (15 February), pp. 4237-42400

Hawrylak, P. & Potemski, M. (1997). Theory of photoluminescence from an interacting two-dimensional electron gas in strong magnetic fields, *Physical Review B* , Vol.65, No.19 (15 November) pp.12386-12384

Hirose, K. & Wingreen, N. S. (1999). Spin-density-functional theory of circular and elliptical quantum dots, *Physical Review B,* Vol.59, No. 7, (15 February) pp. 4604

Jacak, L.; Hawrylak, P. & Wojs, A. (1998)Quantum dots (Springer, Berlin, p. 176)

Hessman, D.; Persson, J.; Pistol, M-E.; Pryor, C.& Samuelson, L. (2001). Electron accumulation in single InP quantum dots observed by photoluminescence *Physical Review B* Vol.64, pp. 233308-1-11

Hosaka, N. & Saiki, T. (2001) Near-field fluorescence imaging of single molecules with spatial resolution in a range of 10 nm, *Journal of Microscopy,* Vol.202 No.2 (May), pp.362-364

Huang, K.& Rhys, A. (1950). Theory of light absorption and non-radiative transitions in F-centers, *Proceedings of the Royal Society of London. Series A, Mathematical and Physical Sciences,* Vol.204, No. 1078 (22 December), pp. 406-423

Ilani, S.; Martin, J.; Teitelbaum, E.; Smet, J.H.; Mahalu, D.; Umansky, V. & Yacoby, A. (2004). The microscopic nature of localization in the quantum Hall effect, *Nature*, Vol.427, (22 December) pp. 328-332

Janssens, K. L.; Partoens, B. & Peeters F. M. (2003). Effect of strain on the magnetoexciton ground state in InP/GaxIn1ÀxP quantum disks *Phisical Review B* Vol.67, pp.235325-8

Kalliakos, S. Rontani, M. Pellegrini, V. GARC´IA, C. P. Pinczuk, A. Goldoni, G. Molinari, E. N. Pfeiffer, L. West K. W. (2008) A molecular state of correlated electrons in a quantum dot *Nature Physics* 4 469

Kastner, M.A. (1993). Artificial atoms, *Physics Today*, (January) pp.24-31

Kukushkin, I. V.; Klitzing, K. von; Ploog, K. & V. B. Timofeev (1989). Radiative recombination of two-dimensional electrons in acceptor δ-doped GaAs-$Al_xGa_{1-x}As$ single heterojunctions, *Physical Review B,* Vol.40, No.11, (15 October) pp.7788-7792

Laughlin, R.B. (1983). Quantized motion of three two-dimensional electrons in a strong magnetic field, *Physical Review,* Vol.27, No.6, (15 March) pp. 3383-3389.

Lewis, A.; Isaacson, M.; Harootunian, A. & Muray, A. (1984). Development of a 500 Å spatial resolution light microscope: I. light is efficiently transmitted through λ/16 diameter apertures, *Ultramicroscopy,* Vol. 13, pp.227-232

Maksym, P.A.; Imamura, H.; Mallon, G.P. & Aoki, H. (2000). Molecular aspects of electron correlation in quantum dots, *Journal of Physics: Condensed. Matter,* Vol.12, R299-334

Maksym, P. A. (1996). Eckardt frame theory of interacting electrons in quantum dots, *Physical Review B,* Vol. 53, No. 16 (15 April) pp.10871-10886

Maleinsky P, Lai C W, Bodalato A, and Imamoglu, A. (2007). Nonlinear dynamics of quantum dot nuclear spins, *Physical Review B,* Vol.75, 035409-7

Matsuda, K.; Matsumoto, T.; Saito, H.; Nishi, K.& Saiki, T. (2000). Direct observation of variations of optical properties in single quantum dots by using time-resolved near-field scanning optical microscope *Physica E,* Vol.7, No.3-4, (May), pp.377-382

Matsuda, K.; Saiki, T.; Nomura S., Mihara, M.; Aoyagi, Y.; Nair S. & Takagahara, T. (2003) "Near-Field Optical Mapping of Exciton Wave Functions in a GaAs Quantum Dot" *Phys. Rev. Lett.* Vol.91, No.17 (24 october), pp.177401-4

Mintairov, A. M.; Kosel, T. H.; Merz, J. L.; Blagnov, P. A.; Vlasov, A. S.; Ustinov, V. M. &Cook, R. E. (2001). Near-Field Magnetophotoluminescence Spectroscopy of Composition Fluctuations in InGaAsN, *Physical Review Letters,* Vol.87, No.27 (31 December), pp.277401-14

Mintairov, A. M.; Sun, K.; Merz, J. L.; Li, C.; Vlasov, A. S.; Vinokurov, D. A.; Kovalenkov, O. V.;Tokranov, V. & Oktyabrsky, S. (2004). Nanoindentation and near-field spectroscopy of single semiconductor quantum dots, *Physical Review B,* Vol.69, No.15 (15 April), pp.155306-12

Mintairov, A. M.; Herzog, J.; Kuno, M. & Merz, J. L. (2010). Near-field scanning optical microscopy of colloidal CdSe nanowires, *Phys. Status Solidi B* Vol.247, No. 6, pp.1416–1419

Nash, K. J.; Scolnick, M. S.; Saker, M. K. & Bass, S. J. (1993). Many Body Shakeup in Quantum Well Luminescence Spectra, *Phys. Rev. Lett.* Vol.70, No.20 (17 May), pp.3115-3118

Oosterkamp, T. H.; Janssen, J. W.; Kouwenhoven, L. P.; Austing, D. G.; Honda, T.& Tarucha, S. *(*1999). Maximum-Density Droplet and Charge Redistributions in Quantum Dots at High Magnetic Fields, *Physical Review Letters,* Vol. 82, No.14 (5 April) pp.2931-2934

Ortner, G.; Bayer, M.; Larionov, A.; Timofeev, V. B.; Forchel, A.; Lyanda-Geller, Y. B.; Reinecke, T. L.; Hawrylak, P.; Fafard, S. & Wasilewski, Z. (2003). Fine Structure of Excitons in InAs/GaAs Coupled Quantum Dots: A Sensitive Test of Electronic Coupling, *Physical Review Letters,* Vol.90, No.8, (28 February) pp. 086404-4

Otsu, M. (1998) Near-Field Nano/Atom Optics and Technology, *Springer-Verlag, Tokyo.*

Paskov, P.P.; Holtz, P.O.; Wongmanerod, S.; Monemar, B.; Garcia, J.M.; Schoenfeld, W.V.& Petroff, P.M. (2000). Auger processes in InAs self-assembled quantum dots, *Physica E*, Vol.6, 440-443

Pohl, D. W.; Denk, W. & Lanz, M. (1984). Optical stethoscpy: Image recording with resolution $\lambda/20$, *Applied Physics Letters,* Vol.44, No.&, (1 April), pp.651-653

Pryor, C.; Pistol, M-E. & Samuelson, L. (1997) Elecronic structure of strained InP/$Ga_{0.51}In_{0.49}$P quantun dots. *Physical Review B,* Vol.56, No.16, (October 15) pp. 10404-10411

Pudalov, V.M.; D'Iotio, M.; Kravchenko, S.V.& Campbell J.W. (1993) Zero-Magnetic-Field Collective Insulator Phase in a Dilute 2D Electron System, *Physical Review Letters*, Vol.70, No.12, (22 March) pp. 1866-1869

Reddick, R. C.; Warmack, R. J. & Ferrell, T. L. (1989). New form of scanning optical microscopy, *Physical Review B,* Vol.39, No.1, (1 January), pp. 767-770

Reimann, S. M.; Koskinen, M. &. Manninen, M. (2000). Formation of Wigner molecules in small quantum dots, *Physical Review B* Vol.62, No.12 (15 September) pp.8108-8113

Reimann, S.M. & Manninen, M. (2002). Electronic structure of quantum dots, *Review of Modern Physics*, Vol.74, No.4, (October), pp.1283-1342

Ren, H.-W.; Sugizaki, M.; Lee, J.-S.; Sugou, S.&Masumoto, Y.,Highly Uniform and Small InP/GaInP Self-Assembled Quantum Dots Grown by Metal-Organic Vapor Phase Epitaxy (1999) *Japanese Journal of Applied Physics* Vol.38, No.1B, Part 1 (January) pp. 507-510

Saint Jean, M; Even, C. & Guthmann, C. (2001). Macroscopic 2D Wigner islands, *Europhysics Letters,* Vol.55, No.1 (1 July), pp. 45–51

Singha A, V. Pellegrini, A. Pinczuk, L. N. Pfeiffer, K. W. West, and M. Rontani, (2010)Correlated Electrons in Optically Tunable Quantum Dots: Building an Electron Dimer Molecule *Phys. Rev. Lett.* 104, 246802

Sugizaki, M.; Ren, H.-R.; Nair, S. V.; Nishi, K&Masumoto, Y. (2002) External-field effects on the optical spectra of self-assembled InP quantum dots. *Physical Review B,*Vol.66, pp.235309-1-10

Synge, E. H. (1928). A suggested method for extending microscopic resolution into the ultra-microscopic region, *Phyloofical Maazine Series 7,* Vol.6, No.35, pp.356-362

Szabo, A. & Ostlund, N. (1996) Modern Quantum Chemistry, *Dover, New York*

Szafran, B.; Bednarek, S. & Adamowski, J. (2003). Magnetic-field-induced phase transitions in Wigner molecules, *Journal of Physics: Condensed Matter*, Vol.15, pp.4189-4205.

Tratakovskii, A. I.; Wright, T.; Russell, A.; Fal'ko, V. I.; Van'kov, A. B.; Skiba-Szymanska, J.; Drouzas, I.; Kolodka, R. S.; Skolnik, M. S.; Fry, P. W.; Taharaoui, A.; Lui, H-Y. & Hopkinson, M. (2007). Nuclear Spin Switch in Semiconductor Quantum Dots, *Physical Review Letters,* Vol.98, No.2 (12 January) pp. 026806-4

Tarucha, S.; Austing, D.G.; Honda, T.; Van der Hage, R.J.; Kouwenhoven, L.P. (1996). Shell Filling and Spin Effects in a Few Electron Quantum Dots, *Physical Review Letters*, Vol.77, No.17 (21 October), pp.3613-3616

Toda, Y.; Kourogi, M.; Otsu, M.; Nagamune, Y.& Arakawa Y. (1996). Spatially and spectrally resolved imaging of GaAs quantum-dot structures using near-field optical technique, *Applied Physics Letters* Vol.69, No.6, (5 August) pp.827-829

Toda, Y.; Shinomori, S.; Suzuki, K. & Arakawa, Y. (1998). Polarized photoluminescence spectroscopy of single self-assembled InAs quantum dots, *Physical Review B*, Vol.58, No.16 (15 October) pp.R10147-10150

Toda, Y.; Sugimoto, T.; Nishioka, M. & Arakawa, Y. (2000). Near-field coherent excitation spectroscopy of InGaAs/GaAs self-assembled quantum dots, *Applied Physics Letters* Vol.76, No.26 (26 June) pp.3887-3889

Toda, Y.; Moriwaki, O.; Nishioka, M. & Arakawa, Y. (1999). Efficient Carrier Relaxation Mechanism in InGaAs/GaAs Self-Assembled Quantum Dots Based on the Existence of Continuum States, *Phys. Rev. Lett.* Vol.82, No.20 (17 May) pp.4114-4117

Vinokurov, D. A.; Kapitonov, V. A.; Nikolaev, D. N.; Sokolova, Z. N. & Tarasov I. S. (1999). Self-organized nanoscale InP islands in an InGaP/GaAs host and InAs islands in an InGaAs/InP, *Semiconductors,* Vol.35, No.7, (July) pp.788-791

Yannouleas, C. & Landman, U. (2000). Collective and Independent-Particle Motion in Two-Electron Artificial Atoms *Physical Review Letters,* Vol.85, No.8, (21 August) pp.1726-1729

Wigner, E.P. (1934) On the Interaction of Electrons in Metals, *Physical Review*, Vol.46, (1 December), pp.1002-1011.

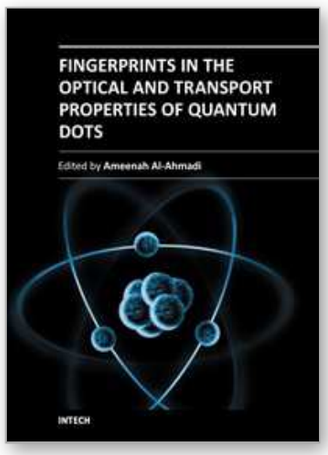

Fingerprints in the Optical and Transport Properties of Quantum Dots

Edited by Dr. Ameenah Al-Ahmadi

ISBN 978-953-51-0648-7
Hard cover, 468 pages
Publisher InTech
Published online 13, June, 2012
Published in print edition June, 2012

The book "Fingerprints in the optical and transport properties of quantum dots" provides novel and efficient methods for the calculation and investigating of the optical and transport properties of quantum dot systems. This book is divided into two sections. In section 1 includes ten chapters where novel optical properties are discussed. In section 2 involve eight chapters that investigate and model the most important effects of transport and electronics properties of quantum dot systems This is a collaborative book sharing and providing fundamental research such as the one conducted in Physics, Chemistry, Material Science, with a base text that could serve as a reference in research by presenting up-to-date research work on the field of quantum dot systems.

How to reference

In order to correctly reference this scholarly work, feel free to copy and paste the following:

Alexander M. Mintairov, James L. Merz and Steven A. Blundell (2012). Molecular States of Electrons: Emission of Single Molecules in Self-Organized InP/GaInP Quantum Dots, Fingerprints in the Optical and Transport Properties of Quantum Dots, Dr. Ameenah Al-Ahmadi (Ed.), ISBN: 978-953-51-0648-7, InTech, Available from: http://www.intechopen.com/books/fingerprints-in-the-optical-and-transport-properties-of-quantum-dots/molecular-states-of-electrons-in-quantum-dots-emission-of-single-molecules-in-self-organized-inp

INTECH
open science | open minds

InTech Europe
University Campus STeP Ri
Slavka Krautzeka 83/A
51000 Rijeka, Croatia
Phone: +385 (51) 770 447
Fax: +385 (51) 686 166
www.intechopen.com

InTech China
Unit 405, Office Block, Hotel Equatorial Shanghai
No.65, Yan An Road (West), Shanghai, 200040, China
中国上海市延安西路65号上海国际贵都大饭店办公楼405单元
Phone: +86-21-62489820
Fax: +86-21-62489821

IntechOpen